scientific reports

Check for updates

OPEN

Numerical analysis of the effect of vegetation root reinforcement on the rainfall-induced instability of loess slopes

Kunfeng Kong[1,2,4], Zixuan Deng[3,4]✉, Feng Chen[1,2], Zheng Wang[3] & Yiling Chen[3]

Rainfall-induced instability of loess slopes presents significant threats to infrastructure and ecological systems. Vegetation serves as an effective measure to enhance slope stability through mechanical reinforcement by roots and hydrological regulation of soil moisture. The influence of vegetation root system characteristics, including root tensile strength and rooting depth, on the stability of loess slopes subjected to rainfall infiltration is investigated using a finite element model developed in COMSOL®, which couples seepage and mechanical behavior. Rainfall infiltration, pore water pressure evolution, and progressive slope failure are simulated to analyze the stability response. Varying levels of additional cohesion provided by roots and different rooting depths are systematically evaluated. The results indicate that stronger root systems and deeper rooting depths significantly enhance slope stability by increasing the factor of safety, delaying plastic zone development, and reducing displacement. The reinforcement effect becomes more pronounced on steeper slopes, while its marginal contribution diminishes with increasing root depth beyond a certain threshold. These findings provide insights into the role of vegetation in mitigating rainfall-induced slope failures and provide practical guidance for the selection and application of vegetation in ecological slope stabilization projects.

Keywords Loess slopes, Rainfall infiltration, Reinforcement of vegetation, Numerical simulation, Stability analysis

Abbreviations

VG	Van Genuchten
SWCC	Soil water characteristic curve
FOS	Factor of safety

Rainfall infiltration increases pore water pressure within soil masses and gradually dissipates the matric suction of unsaturated soils, making it one of the most critical triggers for landslide events[1–6]. Loess, a sediment formed under arid to semi-arid conditions, exhibits a highly porous structure, well-developed vertical jointing, and elevated silt content. It is widely distributed in northwestern China and, as a typical unsaturated soil, demonstrates pronounced hydro-sensitivity and collapsibility. Under intense rainfall, it becomes highly susceptible to geological hazards such as landslides and collapses, which pose significant threats to human safety, property, and infrastructure stability.

Vegetation serves as a natural and effective solution for mitigating slope instability. Through mechanical reinforcement by roots and hydrological regulation of soil moisture, vegetation increases soil cohesion, maintains matric suction, and delays the onset of failure[7,8]. These processes not only improve the soil's resistance to failure but also help reduce surface runoff and soil erosion on steep slopes, as confirmed by both experimental and field studies[9,10]. The growth and proliferation of root systems enhance soil shear strength and structural integrity[11] while also modulating soil moisture through water absorption and retention. This dual function optimizes permeability characteristics and effectively reduces landslide risks during rainfall. Therefore, the

[1]Railway Engineering Research Institute, China Academy of Railway Sciences, Beijing 100081, China. [2]State Key Laboratory of High-Speed Railway Track System, China Academy of Railway Sciences, Beijing 100081, China. [3]School of Civil Engineering, Central South University, Changsha 410075, China. [4]Kunfeng Kong and Zixuan Deng contributed equally to this work. ✉email: dengzx@csu.edu.cn

strategic application of plant root systems presents substantial potential for slope reinforcement and ecological restoration in loess regions.

Many studies confirm that plant roots enhance soil shear strength and significantly contribute to mechanical slope stabilization. Chaobo et al.[12] and Zhang et al.[13] showed that the root systems of Robinia pseudoacacia and Pinus tabuliformis improve shear resistance in loess soils, with added cohesion affected by root diameter and orientation. Pallewattha et al.[14] further highlighted that the mechanical reinforcement provided by roots depends on both soil suction and root failure modes, based on direct shear tests. Grass and shrub roots have also been investigated: Liu Yabin et al.[15] and Zheng Mingxin et al.[16] conducted tensile and pull-out tests, respectively, indicating that root tensile strength and the growth stage of roots affect their reinforcing potential. However, most studies focus on individual species or isolated mechanical factors, with limited evaluation of root reinforcement under varying slope angles and rainfall intensities. In particular, the interaction between root properties and infiltration-induced stress variations remains insufficiently explored.

Root systems also play a vital role in regulating soil moisture and minimizing erosion during rainfall. Wu Hongwei[17] indicated that transpiration-induced suction and root structure help reduce pore pressure and shallow failures. Huang et al.[18] demonstrated, through large-scale slope modeling, that vegetation alters water pathways and increases erosion resistance on steep slopes. These results confirm that, beyond mechanical anchorage, roots mitigate rainfall-induced slope failure by improving infiltration patterns and maintaining unsaturated conditions. However, most investigations examine vegetation's hydrological effects separately from mechanical responses, lacking full coupling under dynamic rainfall. This separation limits the accurate prediction of slope behavior during extended or heavy storms.

Recent modeling efforts aim to integrate the mechanical and hydrological effects of vegetation into slope stability analysis. Li Guorong et al.[19] and Li et al.[20] employed finite element methods to simulate the influence of root systems on slope strength and pore pressure distribution. Feng et al.[11] and Świtała et al.[21] incorporated coupled hydro-mechanical formulations in unsaturated soils, while Cislaghi et al.[22] linked root spatial density from field surveys to numerical models for vineyards. Huang Jiankun et al.[23] and Chen et al.[24] developed advanced constitutive or optimization-based models to represent root-soil composites and analyze dynamic slope response.

Variations in root morphology, including type, depth, and spatial distribution, significantly influence reinforcement effects. Studies by Zhou Xia et al.[25], Xu Tong et al.[26], and Yabin et al.[15] showed that root length, diameter, and tensile strength vary across species and developmental stages, affecting both reinforcement depth and magnitude. Shrub and herbaceous species provide different anchorage patterns, and their interaction with soil depends on local geometry and loading conditions. These insights highlight the importance of selecting appropriate vegetation types for targeted slope conditions. The effects of root traits on slope stability across rainfall and slope conditions remain insufficiently compared, particularly in collapsible loess. How root characteristics scale to overall stabilization is still not well quantified.

Several studies have specifically addressed the influence of rainfall infiltration on root-soil interactions. Guo et al.[27], Zhong Caiyin et al.[28], and Chen et al.[24] developed three-dimensional models to simulate pore water pressure evolution under various rainfall conditions and root distributions. Their findings confirmed that root water uptake delays saturation and helps maintain slope stability under prolonged rainfall, particularly in unsaturated loess. These results highlight the importance of considering root-soil-hydrology coupling in stability analysis under natural rainfall events.

Although vegetation generally improves slope stability, some studies have also identified potential negative effects[29–31]. Inappropriate root system configurations, overly dense shallow roots, or unsuitable species can lead to pore pressure concentration or weakening of surface layers during intense rainfall. Recent studies demonstrate that in sand slopes, vegetation can enhance the factor of safety by up to 34.3%, while in silt slopes the improvement is only a fraction of that, and in clay slopes, vegetation reinforcement can be negligible or even detrimental under certain conditions. Specifically, vegetation-induced surcharge and limited deep rooting in clay soils can counteract stabilizing effects, occasionally leading to reduced stability[31]. These findings emphasize the necessity of site-specific assessments of vegetation types and soil conditions in ecological slope design.

Accordingly, although extensive research exists, a fully integrated understanding of how vegetation characteristics and rainfall jointly influence loess slope stability remains lacking, highlighting the need for more comprehensive hydro-mechanical analyses under variable environmental conditions. Based on these research gaps, this study develops a fully coupled hydro-mechanical numerical model to investigate rainfall-induced instability of loess slopes and the stabilizing effects of vegetation root systems. The model integrates rainfall infiltration processes, root mechanical reinforcement, and water uptake dynamics, allowing for a more realistic simulation of root-soil–water interactions under varied slope and climatic conditions. This study quantitatively assesses the role of vegetation in enhancing slope stability and identifies the conditions under which vegetation reinforcement becomes less effective or even detrimental by systematically varying root tensile strength, rooting depth, slope angle, and rainfall intensity. The results provide theoretical insight and practical reference for vegetation-based slope protection strategies in loess regions.

Methodology

Rainfall effect mechanism

Numerical simulation of rainfall infiltration typically requires the consideration of complex interactions between water flow and soil, involving the coupling of seepage and mechanical analyses. In mechanical analysis, the total stress distribution of the soil σ is combined with the pore water pressure u to compute the effective stress, which serves as the basis for evaluating soil deformation, stress, and shear strength. The mechanical behavior of the soil follows the stress equilibrium equation, given as follows:

$$\nabla \cdot \sigma + f = 0 \tag{1}$$

where ∇ is a differential operator acts on a second-order tensor, $\boldsymbol{\sigma}$ is the stress tensor, and f is the body force vector (external force per unit volume), with both deformation and stress being determined based on the soil's constitutive model.

The Richards equation, or the unsteady-state Darcy equation, is generally employed to describe water movement within the soil and to obtain parameters such as hydraulic head, permeability coefficient, and pore water pressure to analyze seepage in unsaturated soil slopes.

$$\frac{\partial \theta}{\partial t} = \nabla \cdot (k \nabla h) + S \tag{2}$$

where θ is the volumetric water content of the soil, k is the permeability coefficient of unsaturated soil (m/s), h is the pressure head (m), and S denotes the source term. The relationship between matric suction and volumetric water content is described using a soil–water characteristic curve (SWCC) to accurately simulate the unsaturated infiltration process during rainfall events. This study adopts the Van Genuchten (VG) model, which provides a widely accepted empirical formulation for describing unsaturated soils. The VG model[32] is widely employed to represent the SWCC and to describe the underlying mechanisms of soil water transport. In seepage analysis, the model primarily characterizes the variation in soil water saturation under different pressure heads, expressed as follows:

$$\theta = \theta_r + S_e (\theta_s - \theta_r) \tag{3}$$

where θ_s and θ_r are the saturated and residual volumetric water content of the soil, respectively. S_e is the effective saturation, expressed as follows:

$$S_e = [\,1 + (\alpha \mid h \mid)^n\,]^{-m} \tag{4}$$

where α, n, and m are parameters of the VG model. Typically, $m = 1 - \frac{1}{n}$. The parameter α is a constant related to soil particle size and pore structure, controlling the steepness of the soil water retention curve.

Root system mechanism

Mechanical reinforcement

Plant root systems interact with the soil through their fibrous structure, enhancing the shear strength and overall stability of the soil. When vegetation grows on a slope, its roots penetrate and bind soil particles, forming a root-soil composite that increases the soil's tensile and compressive strength. This study applies Wu's model[33] to calculate the additional cohesion provided by vegetation roots, expressed as follows:

$$c_{root} = \lambda \times T_{root} \times R_f \times RAR \tag{5}$$

where c_{root} is the cohesion imparted by the root system (kPa), λ is the correction factor accounting for the effect of gradual root failure on soil shear strength, with a typical value of 0.4[34]. T_{root} is the tensile strength of the plant roots (kPa), which in reality varies with root diameter. This study assumes that all vegetation roots have the same diameter, which simplifies the calculations. *RAR* is the root area ratio, which is defined as the root cross-sectional area per unit of ground surface area. R_f is the root orientation factor[24], which can be defined as follows:

$$R_f = \sin\eta + \cos\eta \tan\phi \tag{6}$$

where η is the angle formed between the vertical direction of the root and the failure plane assumed during root breakage, and ϕ is the internal friction angle of the soil. This study assumes that root failure occurs perpendicular to the slope surface, corresponding to $R_f = 1.0$.

The root reinforcement modeling in this study follows the framework of Wu's model, which estimates the additional shear strength contributed by plant roots. As direct experimental validation of the model lies beyond the scope of this study, parameter values are extracted from existing literature based on typical vegetation types found in loess areas. In particular, the root tensile strength and root area ratio parameters are taken from[35], which examines several forest species in the Alps and Prealps of Lombardy. That study provides tensile strength–diameter relationships and root distribution profiles with soil depth, applicable for slope stability modeling. In this research, Salix purpurea is selected as the representative species. The root tensile strength is set at 51.47 MPa, and the root area ratio is defined as 0.049%, considering variations with depth and root type. These parameters are incorporated into Wu's model to simulate the reinforcement effects of vegetation roots on slope stability.

Hydrological effects

Plant root systems can also improve soil moisture conditions by absorbing and retaining water, reducing the risk of landslides resulting from slope wetting. Compared to unsaturated bare slopes, the seepage and stability analysis of vegetation-covered slopes requires consideration of suction changes caused by transpiration and of the altered soil hydrological properties due to plant influence. Two primary simulation methods are commonly employed to investigate the process by which plants absorb water from the soil through their roots during transpiration: microscopic and macroscopic models. Microscopic models focus on the interactions between individual roots and soil particles within the soil–plant system, considering the water potential of both roots and surrounding soil. These models describe the direction and movement of water through individual roots similarly to Ohm's

law[36]. Although microscopic models provide more accurate predictions of the water absorption process, they are computationally intensive and generally suited to small-scale studies. Therefore, this study adopts a macroscopic model to investigate large-scale vegetation coverage on loess slope surfaces. The soil-vegetation system is treated as a whole. The water absorption by the vegetation roots is considered a source term inserted into the Richards equation, expressed as follows:

$$\frac{\partial}{\partial x}\left(k\frac{\partial h}{\partial x}\right)+\frac{\partial}{\partial y}\left(k\frac{\partial h}{\partial y}\right)-S\left(\psi\right)=\frac{\partial\theta}{\partial t} \tag{7}$$

where ψ is the soil matric suction (kPa). This study applies the source term $S(\psi)$ in the Richards equation, representing root water uptake as a depth-dependent function. The spatial distribution of water uptake by plant roots follows the Feddes model[37], which considers both soil water availability and root distribution with depth. The water absorption source term by the vegetation is expressed as follows[14]:

$$S\left(\psi\right)=F\left(\psi\right)\,G\left(H\right)\,T_p \tag{8}$$

where T_p is the potential transpiration rate of the plant roots (m/s), $G(H)=1/H_1$ is a function utilized to describe the morphology of plant roots, where H_1 is the root depth (m), and the root water absorption reduction function $F\left(\psi\right)$[37] is described as follows:

$$F\left(\psi\right)=\begin{cases}\frac{\psi}{\psi_{an}} & \psi<\psi_{an}\\ 1 & \psi_{an}\le\psi<\psi_d\\ \frac{\psi_w-\psi}{\psi_w-\psi_d} & \psi_d\le\psi<\psi_w\\ 0 & \psi_w\le\psi\end{cases} \tag{9}$$

where ψ_{an} is the critical matric suction (kPa) for oxygen stress in the soil, ψ_d is the critical matric suction (kPa) for water stress in the soil, and ψ_w is the soil suction (kPa) corresponding to the plant wilting point, beyond which the plant begins to enter an irreversible wilting state, and the roots are unable to continue absorbing water from the soil.

Finite element model and stability analysis

This study develops a numerical model to analyze the stability of vegetation-covered loess slopes under rainfall infiltration conditions, incorporating both geometric characteristics and material properties of the slope. The model consists of two primary components: the solid mechanics module and the Darcy's law module. The solid mechanics module simulates the mechanical behavior of the slope, including soil stress, deformation, and the reinforcing influence of vegetation roots. The Darcy's law module models rainfall infiltration and root water absorption, capturing water movement through unsaturated soil. The Mohr–Coulomb constitutive model describes the mechanical properties of the loess slope's soil and rock mass, while the Richards equation governs fluid flow in variably saturated porous media, accounting for nonlinear flow dynamics.

Slope geometrical model

The numerical analysis model for the stability of vegetation-covered loess slopes under rainfall infiltration conditions primarily comprises three components: the soil and rock mass of the loess slope, the surface vegetation-covered zone, and the rainfall infiltration boundary conditions. These components are integrated and coupled within the numerical simulation software COMSOL Multiphysics and applied to analyze loess slope stability.

The soil and rock mass of the loess slope is divided into root and non-root zones by assigning different material properties. The surface vegetation-covered zone is located above the slope surface, with a uniform thickness, using enhanced soil mechanical and permeability parameters, and considering both mechanical reinforcement and hydrological effects. Volumetric water content and matric suction are monitored at locations marked in Fig. 1a, with monitoring points A, B, and C at the slope shoulder, D, E, and F at the slope waist, and G and H at the slope toe. Figure 1a indicates that monitoring points are organized into three groups located at the slope crest, mid-slope, and toe. Within each group, points are vertically distributed below the slope surface at 1.5 m intervals, covering both vegetation-reinforced and rootless zones. This layout enables detailed observation of infiltration dynamics and mechanical responses across different slope zones.

A mesh sensitivity analysis is conducted using three global mesh schemes to evaluate the influence of mesh size on simulation accuracy and computational efficiency: coarse (element size 2 / minimum size 0.01), medium (1.2 / 0.0045), and fine (0.5 / 0.001). The analysis focuses on the factor of safety (*FOS*), pore water pressure, degree of saturation, and infiltration calculation time after 50 h of rainfall. Results show that all three mesh schemes produce comparable *FOS* values (ranging from 1.1775 to 1.19), indicating convergence in overall slope stability. However, the medium mesh captures pore pressure and saturation distribution more accurately than the coarse mesh, particularly in critical zones such as the root zone and slope toe, while avoiding the high computational cost of the fine mesh (100 s vs. 1098 s).

In addition, based on the selected medium mesh, a locally refined mesh is developed to enhance simulation accuracy in critical areas while maintaining computational efficiency. The local refinement primarily targets the slope surface, the vegetation root zone, and regions expected to exhibit steep hydraulic gradients during rainfall infiltration. Compared to the fully fine mesh, the locally refined mesh achieves a similar level of accuracy in terms of pore water pressure and saturation distribution while significantly reducing computation time from

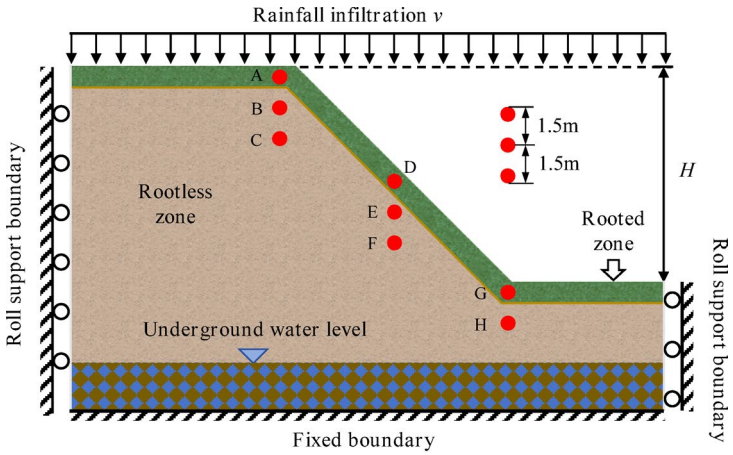

(a)

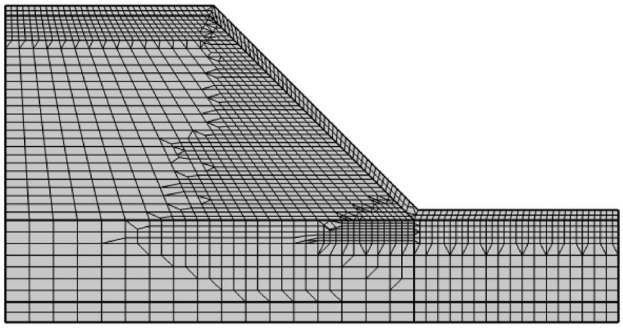

(b)

Fig. 1. (**a**) Slope geometry model and measurement point setting schematic. Points are distributed at the crest, mid-slope, and toe, with a vertical spacing of 1.5 m, covering both the vegetation-reinforced zone and the rootless zone. (**b**) Optimized mesh configuration with medium global density and local refinement in critical zones.

1098 to 844 s. This indicates that local refinement effectively balances the need for detailed resolution in sensitive areas with overall computational cost. Therefore, the final mesh configuration adopts a medium-density global mesh combined with targeted local refinements, as shown in Fig. 1b.

Rainfall infiltration-stress-deformation coupling of unsaturated soil slopes

Rainfall infiltration leads to changes in the volumetric water content of the soil and rock mass, which in turn affect both the sliding force and the self-weight stress acting on the slope. In addition, variations in volumetric water content cause changes in matric suction within the soil layers, which subsequently influence the effective stress acting on the slope. As water infiltrates the soil and rock mass, a seepage field forms. The slope's soil deforms due to the combined effects of loading and seepage, generating a stress field. These two fields interact and influence each other until they reach an equilibrium state. The changes in self-weight stress and effective stress in the model during the rainfall infiltration process are considered key factors influencing slope stability. Based on this model, the effects of self-weight stress and effective stress variation under rainfall infiltration are incorporated to establish a numerical analysis model for the stability of loess slopes subjected to rainfall infiltration.

In the above elastoplastic model, a new set of solid mechanics and Richards equation interfaces is added to simulate the working conditions of rainfall infiltration in loess slopes. In the newly integrated Richards equation module, the surface rainfall inlet of the slope's soil and rock mass is defined. The rainfall infiltration rate in the Richards equation module is expressed by the normal flow velocity. This allows for the calculation of the saturation, displacement, stress, and equivalent plastic strain distributions in the loess slope under continuous rainfall infiltration conditions, providing dynamic monitoring of the moisture infiltration process. It captures the spatial and temporal variations in water content and provides a quantitative analysis of the seepage and

stress system responses of the loess slope, considering various influencing factors such as slope angle and rainfall intensity.

Both the soil–water characteristic and the permeability function curves in this model are derived from the Van Genuchten model[32]. In the COMSOL Multiphysics Richards equation interface, user-defined functions simulate both the reinforcing effect of vegetation roots on soil stability and the impact of plant transpiration on water movement. The governing equation is as follows:

$$\frac{\partial}{\partial t}(\theta_s \rho) + \nabla \cdot (\rho u) = Q_m \tag{10}$$

$$\frac{\partial}{\partial t}(\theta_s \rho) = \rho \left(S_e S + \frac{C_m}{\rho g} \right) \frac{\partial p}{\partial t} \tag{11}$$

$$u = -\frac{K_s k_r}{\rho g}(\nabla p + \rho g) \tag{12}$$

where Q_m is the mass source term, ρ is the density of soil (kg/m^3), p is the pore water pressure (kPa), C_m is the specific volume of water (1/m), S is the storage coefficient (1/Pa), u is the flow velocity vector, g is the gravitational acceleration (m/s^2), K_s is the saturated permeability of the soil (m/s), and k_r is the relative permeability, represented as follows:

$$k_r = S_e \left(1 - \left(1 - S_e^{\frac{1}{m}} \right)^m \right)^2 \tag{13}$$

where m is the fitting parameter of the VG model.

Boundary condition setup

It is assumed in the solid mechanics module that the soil layer is supported by a hard and rough foundation, with fixed constraints applied along the horizontal lower boundary. Roller support boundary conditions are imposed on the vertical boundaries on both the left and right sides of the model, ensuring that horizontal displacement remains zero along these edges. The upper boundary of the model is defined as a free surface, allowing for unrestricted displacement.

Within the Darcy's law module, pressure boundary conditions are applied along the lower sections of the model's left and right sides up to the groundwater level, while all other boundaries are specified as no-flow conditions. A normal inflow velocity is applied on the surface of the loess slope or the vegetation-covered surface, serving as the rainfall infiltration boundary condition.

Calculation of the FOS after rainfall

Based on the previously obtained results, an additional solid mechanics module is introduced to determine the equivalent plastic strain distribution within the slope's rock-soil mass under seepage conditions, using the strength reduction method for analysis.

The finite element method based on strength reduction is a widely accepted approach for assessing slope stability. Its core principle involves solving for the slope's limit state within an elastoplastic finite element model through numerical analysis techniques. Specifically, the method entails the gradual reduction of the strength parameters of the slope's rock-soil mass using numerical software, which leads to a progressive loss of shear resistance until slope failure is achieved. At this point, the strength reduction factor is adopted as the safety factor, representing the remaining strength capacity of the slope. In addition, the software can identify the potential sliding surface of the slope by analyzing the equivalent plastic strain.

The finite element strength reduction method is applied for slope stability analysis using COMSOL Multiphysics. The setup process is as follows: after establishing the loading conditions, the cohesion c and internal friction angle φ are parameterized and defined as functions of the *FOS*, formulated as follows:

$$c_F = \frac{c}{FOS}; \quad \phi_F = \arctan\left(\frac{\tan \phi}{FOS} \right) \tag{14}$$

where c and φ are the actual cohesion and internal friction angle of the soil, c_F and φ_F are the reduced cohesion and internal friction angle of the soil. *FOS* is the reduction factor. Then, utilizing the software's auxiliary scanning function, *FOS* is incrementally adjusted, resulting in a gradual reduction in soil material properties and shear strength until slope instability and failure occur. At this critical stage, the *FOS* represents the slope's stability safety factor, and the corresponding reduced values of c and φ are determined. The possible yield surface is identified by analyzing the equivalent plastic strain contour map derived from the computational results. When the equivalent plastic strain is greater than 0, it indicates that the soil has yielded. Areas with larger equivalent plastic strain exhibit greater plastic deformation in the soil, and therefore, these areas can be utilized to characterize the slip surface of slope instability and failure.

Parameter selection

Based on previously published experimental and numerical studies on loess slope stability, the material parameters employed in this model are listed in Table 1. All parameter values listed in Table 1 are adopted from previously published experimental or numerical studies concerning loess slope stability. Specifically, the

Parameter	Symbol	Value	Parameter	Symbol	Value
Soil density	ρ_s (kg m^{-3})	1600	Cohesion	c (kPa)	25
Saturation moisture content	θ_s	0.35	Friction angle	$\varphi(^\circ)$	20
Residual moisture content	θ_r	0.025	Saturated permeability	K_s (m s^{-1})	5×10^{-6}
Root transpiration rate	T_p (m s^{-1})	1×10^{-6}			

Table 1. Model parameters.

soil physical and mechanical parameters (density, cohesion, friction angle, permeability) are derived from[6,24,38], while the hydraulic parameters and transpiration rate are referenced from root-soil interaction studies such as[28]. Detailed references are provided in the text.

The overall numerical procedure adopted in this study is described as follows: the numerical simulation is conducted in three sequential stages to accurately capture the coupled hydro-mechanical behavior of the slope under rainfall conditions. First, the initial stress field and moisture distribution of the slope are established by applying self-weight loading and solving a steady-state unsaturated seepage problem without rainfall infiltration. The initial hydraulic conditions, including pore water pressure, matric suction, and volumetric water content, are determined based on the SWCC based on the VG model, with a groundwater table specified near the slope toe. Above the groundwater table, the pore water pressure follows a hydrostatic distribution under unsaturated conditions, resulting in a depth-dependent moisture profile where the degree of saturation gradually decreases from near-saturated conditions close to the groundwater table to lower saturation near the slope surface. This approach ensures consistency between the hydraulic and mechanical initial states prior to rainfall infiltration and provides a realistic representation of the natural unsaturated soil condition. The established initial fields are a stable baseline for the following rainfall infiltration analysis.

After establishing the initial conditions, rainfall infiltration is simulated by applying a constant flux boundary condition with a uniform rainfall intensity on the slope surface. The rainfall rate exceeds the soil's saturated hydraulic conductivity to ensure continuous infiltration without immediate surface runoff. No temporal variation in rainfall intensity is considered, and the infiltration boundary remains active for a specified duration to capture the dynamic evolution of pore water pressure, degree of saturation, and stress redistribution within the slope during the rainfall event. During the infiltration stage, a fully coupled hydro-mechanical analysis is performed, simultaneously solving the Richards equation for unsaturated water flow and the mechanical equilibrium equation for soil deformation. A segregated solver strategy is employed within the fully coupled framework, solving the hydraulic and mechanical variables sequentially within each time step until convergence is achieved. A relative convergence tolerance of 10^{-3} is adopted to ensure numerical stability and solution accuracy.

After completing the rainfall infiltration simulation, the final stress and displacement fields are used as initial conditions for the post-rainfall slope stability assessment. The strength reduction method is applied, wherein the shear strength parameters of the soil are gradually reduced until failure occurs, allowing for the calculation of the *FOS* of the slope after rainfall. The failure criterion is defined by either the divergence of the numerical solution or a significant, continuous increase in displacement without achieving equilibrium. This sequential three-stage modeling approach ensures that the transient interactions among rainfall infiltration, pore water pressure evolution, soil deformation, and stability degradation are accurately captured throughout the simulation process. The overall structure of this study is illustrated in Fig. 2.

Results

Rainfall infiltration-induced deformation of loess slopes

Spatial and temporal distribution of moisture content in loess slopes

As rainfall occurs, water infiltrates the soil through its pores, resulting in an increase in moisture content. This process advances further with the continued duration of rainfall, affecting the soil's physical and mechanical properties. Based on the numerical model results of this study, Fig. 3 presents the evolution of the degree of saturation (dimensionless, 0–1) within the slope at different infiltration times (0, 20, 40, and 80 h) under continuous rainfall. Red areas in the figure correspond to lower saturation levels, while blue areas indicate higher saturation levels. The downward movement of the saturation front is clearly observed through the progression of color transitions and contour shifts, indicating the gradual advancement of the wetting front and moisture accumulation within the slope body, particularly in the vegetation-reinforced zones.

The soil surface begins to absorb moisture in the early stages of rainfall. As rainfall continues, water percolates downward, increasing the moisture content of the soil. The distribution of soil moisture following rainfall infiltration reveals that, as time progresses, the initially dry areas gradually become saturated, with the saturated zone continuing to extend deeper into the soil. At different stages of rainfall infiltration, the saturation distribution within the slope exhibits distinct characteristics. During the initial stages of rainfall, the saturated zone is primarily concentrated at the surface. As infiltration time increases, the saturated zone gradually extends deeper, forming a deeper saturated layer. As infiltration time further increases, the unsaturated area gradually decreases, and this reduction corresponds to the natural shape of the slope, indicating that moisture penetration is uniform and thorough.

As soil moisture content increases due to rainfall infiltration, the shear strength of the soil decreases, which heightens the risk of slope failure. Therefore, with the continued infiltration of rainfall over time, the slope's stability is expected to decline, increasing the likelihood of a landslide.

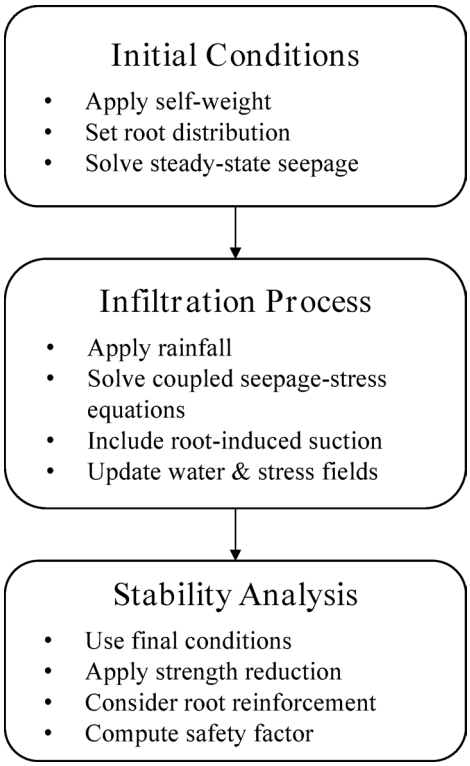

Fig. 2. Framework for assessing the stability of vegetated loess slope.

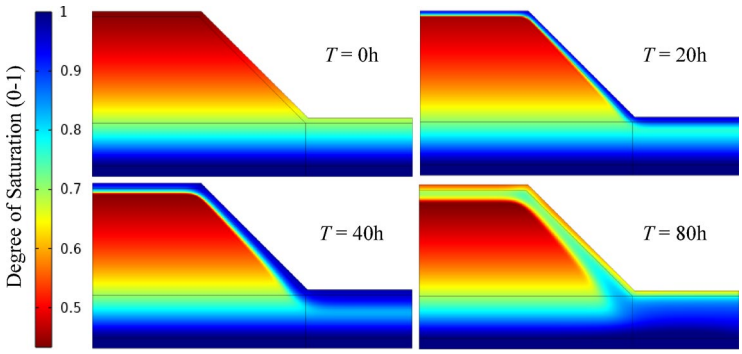

Fig. 3. Saturation distribution contour map of loess slope under diachronic factors.

Figure 4a illustrates the variation in soil volumetric water content at different locations within the slope as the rainfall duration increases, with a constant rainfall intensity of 0.2 m/d. Points A, B, and C represent three locations vertically spaced 1.5 m apart near the top of the slope. From the figure, approximately 3 h after the onset of rainfall, the water content at point A begins to increase. Around 25 h later, the water content at point B starts to rise, while the volumetric water content at point C remains nearly unchanged throughout the 50-h rainfall period. This indicates that the model effectively simulates the gradual filling of soil pore spaces from the top downward.

Before the increase, there is a brief decrease in the soil's volumetric water content, which results from the redistribution of moisture within the soil. After the rainfall begins, water initially infiltrates the upper layers of the soil, while the deeper layers do not absorb any moisture. Hence, the distribution of moisture within the soil changes, leading to a temporary reduction in water content in the deeper layers.

Points D, E, and F are located beneath the slope, and the changes in volumetric water content at these locations exhibit a pattern similar to that of the first three points. Initially, a slight decrease in volumetric water content is observed, followed by a gradual increase as the rainfall continues to infiltrate the soil. The figure also shows that the initial volumetric water content at the top, surface, and base of the slope is not uniformly influenced by the groundwater level. Over time, the rate of increase in volumetric water content at each location gradually slows down, ultimately reaching a saturated water content of 0.35. This confirms that the soil in these areas has attained

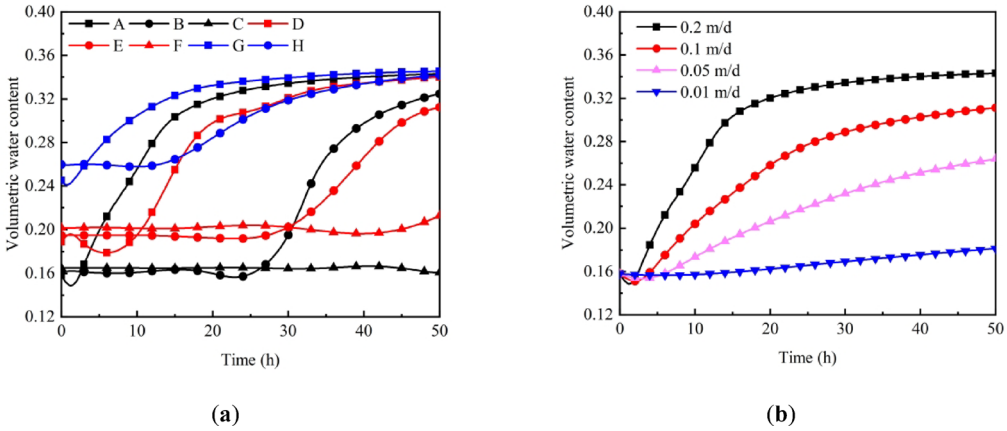

(**a**) (**b**)

Fig. 4. Variation curve of volume moisture content of the loess slope under diachronic factors: (**a**) different locations; (**b**) different rainfall intensities.

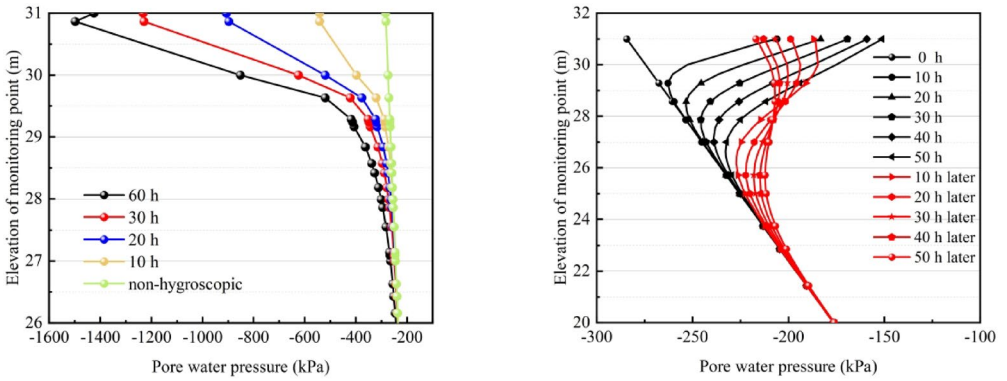

(**a**) (**b**)

Fig. 5. Pore water pressure distribution under continuous rainfall: (**a**) only transpiration; (**b**) rainfall and transpiration.

full saturation, transitioning from an unsaturated to a saturated state. Figure 4b presents the temporal variation of volumetric water content at point A under different rainfall intensities.

In nature, the transpiration rate of plants is relatively low, and its effect on the slope is a long-term process. The transpiration rate is appropriately increased to make the difference in pore water pressure distribution more noticeable. Figure 5a illustrates the temporal variation of pore water pressure in the soil, with the impact of rainfall excluded to provide a clearer understanding of how the root water uptake model influences pore pressure within the slope soil. Over time, a gradual decrease in pore water pressure at the surface is observed. After 60 h of transpiration, the pore water pressure increases by 4.6 times compared to its initial value, highlighting the significant impact of root water uptake. The pore water pressure envelope exhibits a parabolic shape, with the minimum pore pressure occurring in the middle of the root zone.

As rainwater infiltrates, the slope soil becomes progressively saturated from top to bottom. However, the effect of root water uptake reduces the rate at which saturation occurs. Figure 5b illustrates the variation in pore water pressure within the slope soil during the 50 h rainfall period and the subsequent 50 h period after the rainfall ceases. During the first 0 to 50 h, as rainfall infiltrates, the pore water pressure at the slope surface gradually increases. After the rain stops, the pressure begins to decrease steadily, primarily due to the effect of root water uptake. The inflection points of each pore water pressure curve represent the process of moisture front displacement and gradual recovery driven by water forces within the soil. Figure 6 shows the *FOS* of the loess slope at various time intervals, which is calculated using the strength reduction method. Before 50 h, the *FOS* of the slope continually decreases, indicating that rainfall is the primary factor contributing to slope failure. The stability decreases more significantly at the early stage of rainfall and after prolonged exposure. After the rainfall ceases, influenced by water uptake and transpiration, the *FOS* increases, indicating that the slope regains stability.

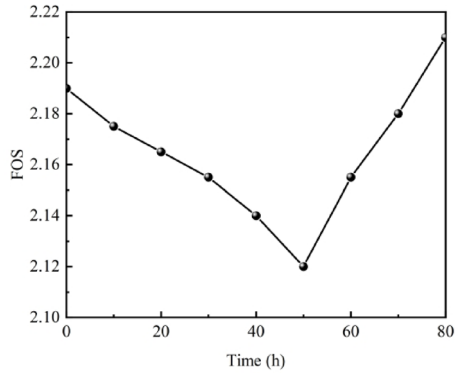

Fig. 6. *FOS* varying with rainfall time.

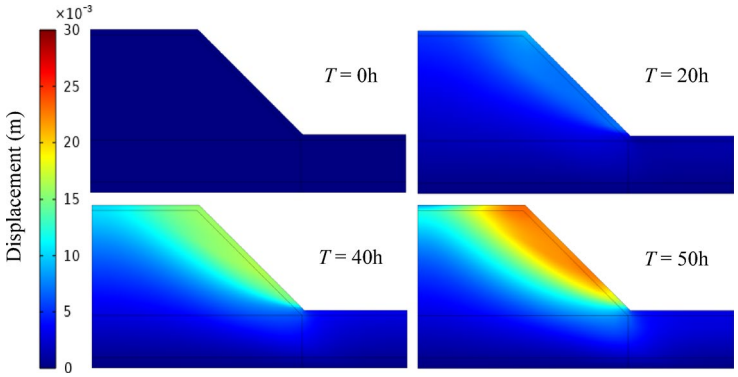

Fig. 7. Displacement distribution of the loess slope under diachronic factors.

Spatial and temporal distribution of displacement in loess slopes

As the rainfall infiltration time accumulates, the stress–strain behavior of the loess slope undergoes a series of complex changes. Rainfall infiltration increases the moisture content of the loess slope soil, elevating the pore water pressure within the slope. This subsequently reduces the soil's effective stress, which in turn diminishes its shear strength and compromises the overall slope stability. Figure 7 illustrates the slope's displacement distribution at different infiltration time intervals (0, 20, 40, and 50 h), as derived from the two-dimensional numerical simulation results.

The stress within the geotechnical body of the slope exhibits a radiating pattern from the interior outward, and with increasing depth, the stress level gradually rises from the surface to the deeper layers, forming a wave-like, layered distribution. Even under the influence of rainfall infiltration, the stress distribution pattern of the slope remains largely consistent with its original state. The comparative analysis reveals that stress concentration primarily occurs at both the slope crest and toe. In addition, the plastic strain distribution map indicates that rainfall infiltration intensifies strain at the slope toe, a phenomenon that aligns closely with the stress distribution patterns observed in the contour analysis.

Stability of loess slopes and analysis of vegetation slope protection effects

This section presents a series of parametric analyses conducted to achieve a more comprehensive understanding of the key factors affecting the stability of vegetated slopes with root reinforcement under unsaturated conditions. The slope stability *FOS* was calculated and compared across various scenarios using the previously discussed strength reduction method. This method facilitated the evaluation of how rainfall infiltration influences slope stability while also examining the contribution of vegetation roots to reinforcing the slope's structural integrity. The parameters considered in this analysis are detailed in Table 1. Figure 8 depicts the simulation results at the critical failure point of the loess slope, depicting the distributions of equivalent plastic strain and displacement. Figure 8a indicates that a continuous high-strain zone develops from the slope surface to the slope toe, indicating the formation of a potential sliding surface. Figure 8b shows the corresponding displacement distribution, where large displacements are concentrated along the same path as the plastic strain zone, further confirming the location and shape of the failure surface. These results show that the slope undergoes progressive failure, characterized by localized plastic deformation and significant displacement accumulation along the critical slip surface.

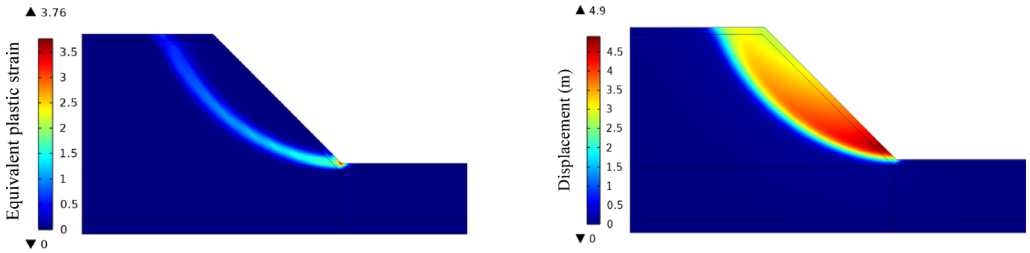

(a) (b)

Fig. 8. Distribution of equivalent plastic strain (**a**) and displacement (**b**) of the loess slope under instability.

Conditions	Slope gradient *I*	FOS_{bare}	FOS_{root}	Conditions	Slope gradient *I*	FOS_{bare}	FOS_{root}
1	1:0.5	1.09	1.2675	5	1:1.5	1.76	1.85
2	1:0.8	1.35	1.4675	6	1:2	2	2.08
3	1:1	1.47	1.59	7	1:3	2.42	2.48
4	1:1.2	1.59	1.7	8	1:5	3.22	3.28

Table 2. *FOS* of the slope under different working conditions.

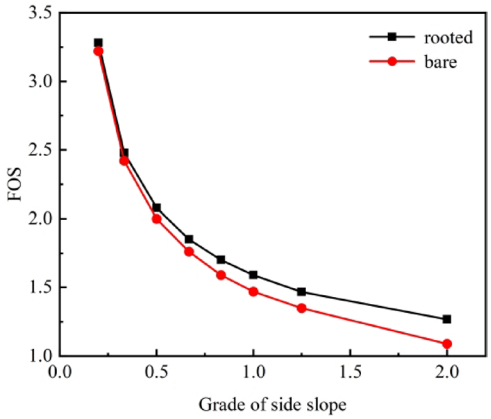

Fig. 9. Effect of slope on *FOS*.

Effect of slope gradient

The increase in slope angle results in a larger component of gravity along the slope direction. As the slope angle increases, the gravitational component of the soil's self-weight also rises along the slope, raising the risk of landslides or soil sliding. Slopes with steeper gradients are more susceptible to sliding under external forces, such as rainfall or earthquakes. The analysis of the slope angle's impact focuses primarily on evaluating how the slope's stability changes at various angles, assessing its susceptibility to instability. This section sets eight different slope angles, with the rainfall duration controlled at 50 h, the infiltration rate at 0.01 m/h, and the vegetation root depth at 1 m. The stability safety factors for both bare and vegetated slopes are calculated using the model, as listed in Table 2.

Figure 9 illustrates the stability of both bare and vegetated slopes under varying slope conditions. The simulation results clearly demonstrate that the slope angle plays a critical role in influencing the *FOS*. Under identical rainfall conditions, steeper loess slopes are more prone to instability. The *FOS* for slopes covered with vegetation is greater than that for bare soil slopes, indicating that the presence of plant root systems contributes to improved slope stability. When the slope is 1:0.5, the *FOS* increases by 16.28% due to vegetation reinforcement, while for a slope of 1:5, the *FOS* increases by only 1.86%. This indicates that as the slope angle increases, the reinforcing effect of vegetation on loess slopes becomes more significant.

Effect of rainfall patterns

The intensity and duration of rainfall affect soil moisture content, soil strength, and groundwater levels, altering slope stability. Intense rainfall rapidly increases soil moisture content, which in turn reduces the shear strength of the soil. This effect is particularly pronounced in regions with steeper slopes, where high-intensity rainfall

quickly saturates the soil, resulting in a significant buildup of pore water pressure and increasing the likelihood of landslides. Intense rainfall typically triggers rapid landslides over a short period, especially in loose or highly permeable soils.

Rainfall duration determines the process of water infiltration and soil saturation. Prolonged rainfall has a cumulative effect on the slope, as it raises groundwater levels and increases the wetting depth of the soil. In regions with high water tables, continuous rainfall enables moisture to penetrate deeper soil layers, increasing the gravitational load on the slope and reducing the soil's shear strength, elevating the risk of instability. Therefore, it is essential to consider rainfall factors when assessing slope stability. Figure 10 illustrates the results of this study, which examined the influence of rainfall duration and intensity on slope stability.

Figure 10 illustrates the stability of both bare soil slopes and vegetated slopes under varying rainfall durations and intensities. The simulation results demonstrate that rainfall conditions significantly affect the *FOS*. As rainfall duration increases, the surface soil of the slope progressively becomes saturated, leading to a reduction in shear strength. This reduction increases the slope's susceptibility to instability. Figure 10a shows the change in *FOS* for slopes with different gradients under continuous rainfall at a rate of 0.01 m/h. Within 100 h, the *FOS* of the bare slope declines from 1.63 to 1.01, a reduction of 38%, while the vegetated slope's *FOS* decreases by only 12.5%. This result shows that the rate of *FOS* reduction is smaller for vegetated slopes under rainfall, indicating that plant roots significantly reinforce the slope. Figure 10b presents the variation in the *FOS* for both bare soil slopes and vegetated slopes under different rainfall intensities. As rainfall intensity increases, slope stability decreases. This finding implies that heavy rainfall or storms serve as significant triggers for landslides. A comparison between the two slope types reveals that, under identical rainfall conditions, the vegetated loess slope exhibits greater stability.

Effect of vegetation reinforcement

Rainfall-induced slope instability results from soil saturation, elevated groundwater levels, and erosive water flows, which collectively reduce soil shear strength and raise mass movement. Vegetation mitigates these destabilizing effects through integrated biomechanical and hydrological mechanisms. Roots mechanically reinforce slopes by binding soil particles and increasing shear resistance through tensile strength, while simultaneously regulating soil hydrology via water uptake, delaying saturation, and the accumulation of pore pressure.

This section investigates the effects of different vegetation types and root depths on slope reinforcement under rainfall conditions, with simulations performed across various scenarios to assess their impact. This study utilizes numerical simulations under controlled rainfall intensity (0.01 m/h) and slope geometry to systematically evaluate how root system characteristics influence these stabilization processes. The analysis quantifies their relative contributions to slope stability by isolating two key variables, vegetation species (determining root tensile strength) and root depth.

This study uses different root tensile strengths to represent various vegetation species applied for slope reinforcement. Based on Eq. (5), a direct relationship is established among vegetation type, planting density (reflected by the root area ratio), and the additional cohesion provided by the root system. Varying levels of additional cohesion are derived by adjusting root tensile strength and the root area ratio, enabling the simulation of different vegetation configurations on the slope surface. Accordingly, setting distinct values of additional cohesion in the model facilitates a realistic representation of various vegetation types and planting strategies commonly implemented in ecological slope stabilization.

Six levels of additional cohesion, 10, 20, 30, 40, 50, and 60 kPa, are selected to systematically investigate the influence of different vegetation types and root system characteristics on slope stability. The root tensile strength and distribution parameters employed in this study are based on empirical data from representative vegetation species commonly found on loess slopes to enhance realism[35,39]. These values correspond to realistic ranges derived from empirical measurements of various vegetation species typically used in ecological slope

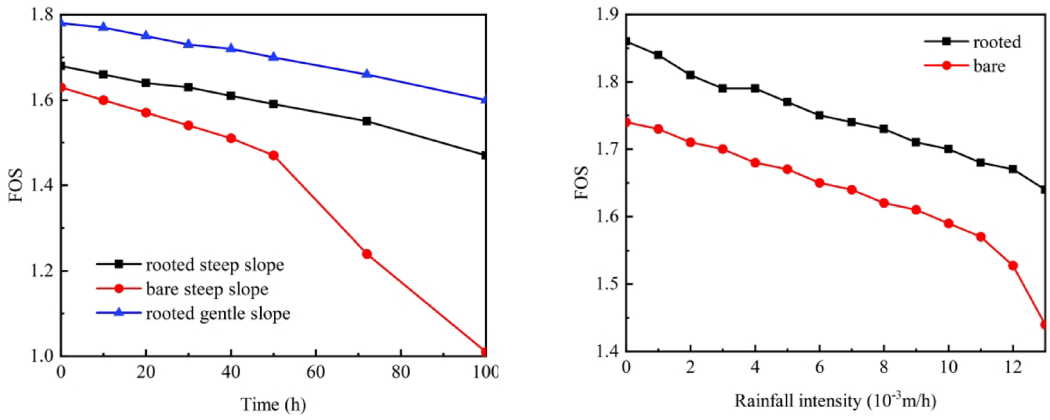

Fig. 10. Influence of rainfall pattern on *FOS*: (**a**) different slope gradients; (**b**) different rainfall intensities.

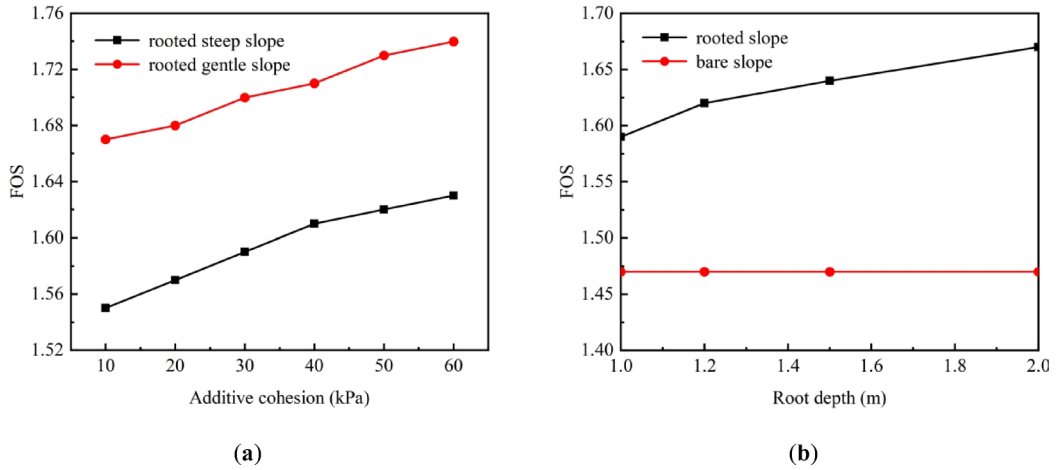

(a) (b)

Fig. 11. Effect of (**a**) vegetation type and (**b**) root depth on *FOS*.

protection, as well as differing root densities. Lower cohesion values (10–20 kPa) represent shallow-rooted grasses or sparsely distributed shrubs, whereas higher values (50–60 kPa) reflect dense-rooted woody plants such as Robinia pseudoacacia or Salix purpurea. This parameterization enables the simulation to capture the variability in vegetation reinforcement capacity across diverse ecological conditions and planting strategies.

The simulation results highlight the critical influence of vegetation characteristics, specifically root tensile strength and root depth, on slope stability under rainfall conditions. Figure 11a illustrates the impact of vegetation type on slope stability. The results show that increasing root tensile strength leads to a marked improvement in the *FOS* and a significant reduction in plastic strain development. Specifically, enhancing the additional cohesion from 10 to 60 kPa results in an approximate 5% increase in the FOS under identical rainfall conditions. An increase in the tensile strength of the root system under the same rainfall conditions leads to greater cohesion provided by vegetation, improving slope stability.

Root depth also plays a vital role. Figure 11b illustrates the effect of root depth on slope stability. As the root depth increases from 1.0 to 1.2 m, the *FOS* rises by 1.89%, and with a further increase to 2.0 m, an additional growth of 3.01% is observed. The *FOS* improves by approximately 4.9% from 1.0 to 2.0 m; however, the rate of improvement diminishes with greater depths, indicating a nonlinear relationship between root depth and slope stabilization effectiveness. Deeper roots contribute to a broader mechanical anchorage zone and enhance the hydrological regulation capacity, effectively delaying pore water pressure buildup and maintaining unsaturated conditions for extended periods.

Quantitatively, enhancing root tensile strength and increasing root depth within a reasonable range can improve the factor of safety by up to 5%, based on the simulation results. Accordingly, the simulation results demonstrate that vegetation significantly enhances slope stability during rainfall infiltration through a combination of biomechanical reinforcement and hydrological regulation mechanisms. An increase in root tensile strength enhances the effective cohesion of the soil mass, delays the onset of plastic deformation, and improves the factor of safety. Deeper root systems provide more effective mechanical anchorage and contribute to improved control of moisture infiltration and pore pressure development. However, the marginal stabilization effect decreases as root depth increases beyond the main critical slip surface. These findings emphasize the importance of selecting vegetation species with high root tensile strength and sufficient root penetration depth to maximize slope reinforcement under rainfall conditions.

Discussion and limitations

This section presents the key findings of the numerical simulations, focusing on the failure mechanisms, vegetation reinforcement effects, and the influence of vegetation characteristics under rainfall infiltration. Each aspect is examined in relation to established theories and prior experimental or numerical studies to validate the reliability and significance of the results. In addition, critical threshold conditions at which vegetation loses its effectiveness are identified and discussed. Finally, the limitations of the current modeling approach and recommendations for future investigations are highlighted.

Validation of predicted failure mechanisms

The numerical simulation outcomes indicate that the failure surfaces initiated by rainfall infiltration are predominantly shallow to intermediate in depth, extending from the slope surface to the toe. The failure mechanism is characterized by the progressive development of localized plastic deformation, followed by significant displacements along a continuous slip zone. This behavior corresponds closely with the findings from field model experiments of rainfall-induced shallow landslides, particularly in loess and other unsaturated soils[40]. The predicted failure patterns indicate that rainfall infiltration plays a primary role in weakening the near-surface soil layers, triggering the initiation and propagation of sliding surfaces under reduced effective stress conditions.

Further analysis of the equivalent plastic strain distributions reveals that initial plastic deformation tends to localize near the slope crest and mid-slope regions, where stress concentrations and moisture accumulation are most significant. As rainfall infiltration continues, these localized plastic zones expand downward and coalesce, eventually forming a continuous potential sliding surface. The displacement field supports this development, with the maximum displacements aligning precisely along the identified plastic strain zones. This progressive failure behavior is typical of rainfall-triggered landslides[41], in which the gradual loss of matric suction and reduction in shear strength lead to a delayed but rapid failure once a critical saturation threshold is exceeded.

The simulation results validate the typical mechanisms of rainfall-induced slope instability, including the transition from localized deformation to a continuous slip surface, and emphasize the importance of monitoring near-surface soil conditions during prolonged rainfall events to anticipate potential slope failures.

Mechanisms of vegetation reinforcement on slope stability

From a mechanical perspective, vegetation roots act as natural reinforcing elements within the soil mass. Roots enhance the apparent cohesion of the soil and improve its shear resistance by physically binding soil particles and bridging potential shear surfaces[42]. The tensile strength of roots introduces an additional stabilizing force that counters gravitational driving stresses, particularly along developing failure planes. The simulation results demonstrate that increasing root tensile strength results in higher factors of safety and a delayed onset of plastic strain zones. This observation aligns with previous experimental and theoretical studies[43], which showed that the mechanical contribution of roots can significantly enhance slope stability, particularly under saturated or partially saturated conditions. The reinforcement effect is especially vital in mitigating shallow failures triggered by rainfall infiltration.

In addition to mechanical reinforcement, vegetation roots significantly influence the hydrological behavior of soil during rainfall events. Root systems enhance water uptake through transpiration and modify infiltration patterns by establishing preferential flow paths and zones of increased matric suction. The simulation results indicate that the presence of roots delays the progression of the wetting front, decreases the rate of pore water pressure accumulation, and preserves higher suction values in the unsaturated soil layers. These hydrological effects effectively extend the soil's resistance to shear failure during rainfall infiltration. Such results highlight the role of vegetation in regulating soil moisture dynamics and reducing the risk of rainfall-induced slope instability.

Influence of vegetation characteristics

Although the general presence of vegetation enhances slope stability, the degree of reinforcement is primarily determined by specific root system characteristics, such as root tensile strength and rooting depth. The numerical simulations presented in this study systematically assessed the influence of these two critical parameters under controlled rainfall infiltration scenarios. The results indicate that variations in root tensile strength and depth markedly affect the factor of safety, deformation behavior, and failure mechanisms of the slope. In addition, the efficiency of vegetation reinforcement declines under extreme slope geometries or intense rainfall conditions, indicating the existence of threshold conditions beyond which vegetation alone cannot effectively stabilize the slope.

The simulation results demonstrate that both root tensile strength and rooting depth are vital in enhancing slope stability during rainfall infiltration. An increase in root tensile strength contributes directly to higher additional cohesion within the soil mass, leading to improved shear resistance and delayed failure onset. Rooting depth also plays a substantial role in influencing slope performance. As the root zone extends deeper into the slope, a larger soil volume benefits from mechanical support and hydrological regulation. However, the rate of stabilization gain decreases with increasing depth, indicating a nonlinear response. This diminishing marginal effect shows that once the primary failure surface is entirely encompassed within the root-reinforced zone, additional root depth provides limited extra stabilization benefits.

Although vegetation substantially improves slope stability under moderate conditions, its effectiveness is reduced beyond specific critical thresholds of slope geometry and rainfall intensity. The simulation results indicate that when the slope angle exceeds a certain threshold, the mechanical reinforcement provided by vegetation roots becomes inadequate to resist the increased gravitational driving forces, resulting in slope failure despite vegetation presence. This critical slope angle varies depending on soil properties and rainfall intensity. This observation aligns with the findings of Simon[44], who reported that vegetation reinforcement becomes less effective on steep slopes due to geometric intensification of destabilizing forces.

Similarly, during high-intensity rainfall events that exceed the soil's infiltration capacity, rapid pore pressure accumulation surpasses the hydrological buffering capability of root systems. In these situations, the soil quickly reaches saturation, and the associated decrease in matric suction causes a sharp reduction in shear strength, triggering slope failure. These results emphasize the need to carefully consider both slope angle and anticipated rainfall conditions when designing vegetation-based slope stabilization strategies, especially in areas vulnerable to extreme weather events.

The numerical simulation results validate classical mechanisms of rainfall-induced slope failure and demonstrate the significant reinforcement effects of vegetation through biomechanical and hydrological processes. The influence of root tensile strength, root depth, and threshold environmental conditions in determining slope stability is systematically analyzed. The findings highlight the importance of optimizing vegetation characteristics to achieve effective slope stabilization while acknowledging the limitations of such reinforcement under extreme geomorphological and climatic conditions. These insights enhance the understanding of vegetation-based stabilization methods and provide a foundation for advancing slope management practices.

Limitations and future work

Although this study provides a preliminary assessment of vegetation-reinforced loess slope stability, certain limitations remain in the current research, necessitating continued improvement in future investigations:

(1) This study only considers the uniform distribution of vegetation roots within the soil mass, whereas real-world environments exhibit more complex spatial distribution patterns[45]. Future research can further optimize root mechanical models, incorporate more complex soil properties, and evaluate the combined effects of various environmental conditions. In addition, more detailed studies on vegetation types and root density can provide more precise guidelines for slope ecological restoration and engineering design.
(2) This study sets the rainfall intensity as a constant in each case; however, the variable rainfall ephemeral function more accurately reflects the actual situation[39]. Therefore, the stability of slopes under variable rainfall intensity will be further examined in future studies.
(3) Although this study aims to capture the representative response of loess slopes reinforced by vegetation, a detailed sensitivity analysis of model parameters will be conducted in future work to assess the robustness of the predicted stability outcomes.
(4) The numerical model in this study is parameterized based on literature values and qualitatively captures the mechanical contribution of vegetation roots. Future efforts will concentrate on conducting direct experimental verification and species-specific parameter calibration.

Conclusions

This study establishes a finite element model of a loess slope and simulates the rainfall infiltration process, exploring the reinforcing effect of vegetation roots on slope stability. It demonstrates the complex interactions among vegetation roots, soil, and rainfall-induced hydrological processes. The findings indicate that vegetation roots significantly enhance slope stability, particularly under rainfall conditions, where the reinforcement effect becomes more evident. The stability of loess slopes improves effectively by appropriately selecting and configuring vegetation, providing a scientific foundation for ecological restoration and disaster prevention.

- Rainfall infiltration has a significant impact on the hydro-mechanical behavior of loess slopes. As rainfall progresses, pore water pressure increases, matric suction dissipates, and the degree of saturation rises, especially in the shallow soil layers. These changes cause a gradual reduction in the soil's shear strength and result in a consistent decrease in the *FOS*. Numerical results show that saturated zones initially develop near the slope toe and crest, gradually expanding inward, while the unsaturated region contracts. This infiltration-driven weakening mechanism serves as a primary cause of rainfall-induced slope instability and must be carefully addressed in slope reinforcement designs.
- Vegetation roots enhance the shear strength of loess slopes by contributing additional cohesion through tensile resistance and interfacial bonding. They reduce soil saturation, delay the onset of instability, and mitigate the risk of sliding. Simulation results show that the tensile strength and rooting depth of vegetation significantly affect slope performance. Deep-rooted vegetation improves slope stability more effectively than shallow-rooted systems. For example, increasing root depth from 1.0 to 2.0 m raised the *FOS* by approximately 4.9%, although the rate of improvement decreased at greater depths. Similarly, under identical rainfall conditions, higher root tensile strength led to a marked increase in additional cohesion and FOS. The stabilizing effect of vegetation becomes increasingly evident on steeper slopes: when the slope ratio was 1:0.5, root reinforcement increased the *FOS* by 16.28%, while the increase is only 1.86% at a slope ratio of 1:5.
- As rainfall progresses, the slope's *FOS* continues to decline. In addition, slope inclination plays a significant role in affecting the *FOS* and influencing overall slope stability. Under identical rainfall conditions, steeper loess slopes exhibit a greater susceptibility to instability. During rainfall infiltration, continuous sliding surfaces and arc-shaped plastic zones emerge within the slope. The maximum strain concentration zone occurs at the slope toe. An arc-shaped sliding surface forms internally, extending throughout the slope, with the displacement direction of the sliding body aligning with the tangent direction of the sliding surface, and a displacement concentration zone appears at the slope toe.

Data availability

The raw data supporting the conclusions of this article will be made available by the corresponding author on reasonable request.

Received: 11 March 2025; Accepted: 9 June 2025
Published online: 02 July 2025

References

1. Wang, S., Idinger, G. & Wu, W. Centrifuge modelling of rainfall-induced slope failure in variably saturated soil. *Acta Geotech.* **16**(9), 2899–2916 (2021).
2. Zhao, N., Lu, H. & Zhang, R. The coupling effect of pore water pressure and pore water gravity in unsaturated soils under rainfall condition and its influence on slope stability. *Geofluids* **2022**(1), 9492514 (2022).
3. Han, J., Zhao, D., Sanqing, S., Xin, M. & Guanbing, L. Analytical solution of rainfall infiltration in homogeneous unsaturated slope andits application in loess slope. *Rock Soil Mech.* **44**(1), 241–250 (2023).
4. Tu, M., Yuan, S., Chen, J. & Ge, Y. Slope stability evaluation of mine rehabilitation project under different rainfall conditions. *Bull. Geol. Sci. Technol.* **43**(6), 63–77 (2024).
5. Li, Z. & Yin, Z. Failure pattern of dispersive soil slopes under the action of rainfall conditions. *Alex. Eng. J.* **104**, 193–210 (2024).
6. Zheng, Y., Wu, H., Luan, X. & McCartney, J. S. Numerical simulation of rainfall-induced deformations of embankments considering the coupled hydro-mechanical behavior of unsaturated soils. *Comput. Geotech.* **175**, 106714 (2024).

7. Lee, E. H. & Sohn, B. J. Examining the impact of wind and surface vegetation on the Asian dust occurrence over three classified source regions. *J. Geophys. Res. Atmos.* **114**(D6) (2009).
8. Ng, C. W. W., Zhang, Q., Ni, J. & Li, Z. A new three-dimensional theoretical model for analysing the stability of vegetated slopes with different root architectures and planting patterns. *Comput. Geotech.* **130**, 103912 (2021).
9. Aqeel, M., Murtaza, N., Ahmed, W., Pasha, G. A., Ghumman, A. R., Ahmed, A. & Zhao, X. Soil erosion on steep hills with varying vegetation patterns. *Phys. Fluids* **37**(1) (2025).
10. Rehman, S. U. et al. A laboratory study of the role of nature-based solutions in improving flash flooding resilience in hilly terrains. *Water* **16**(1), 124 (2023).
11. Feng, S., Liu, H. W. & Ng, C. W. W. Analytical analysis of the mechanical and hydrological effects of vegetation on shallow slope stability. *Comput. Geotech.* **118**, 103335 (2020).
12. Zhang, C. B., Chen, L. H. & Liu, X. P. Tri-axial compression test of loess-root composites to evaluate mechanical effect of roots on reinforcing soil. *J. Soil Water Conserv.* **23**(2), 57–60 (2009).
13. Zhang, C., Chen, L. & Jiang, J. Vertical root distribution and root cohesion of typical tree species on the loess plateau, China. *J. Arid Land* **6**, 601–611 (2014).
14. Pallewattha, M., Indraratna, B., Heitor, A. & Rujikiatkamjorn, C. Shear strength of a vegetated soil incorporating both root reinforcement and suction. *Transp. Geotech.* **18**, 72–82 (2019).
15. Liu, Y., Li, S., Yu, D. et al. Experiment on single root tensile mechanical properties of typical herb species in loess region of Xining Basin (2018).
16. Zheng, M., Huang, G. & Peng, J. Tensile-pullout properties of roots of Magnolia multiflora in different growth stages and stability of slope with its root. *Trans. Chin. Soc. Agric. Eng.* **34**, 175–182 (2018).
17. Ng, C. W. W. Atmosphere-plant-soil interactions: Theories and mechanisms. *Chin. J. Geotech. Eng.* **39**(1), 1–47 (2017).
18. Huang, S. P., Chen, J. Y., Xiao, H. L. & Tao, G. L. Test on rules of rainfall infiltration and runoff erosion on vegetated slopes with different gradients. *Rock Soil Mech.* **44**(12), 3435–3447 (2023).
19. Li, G. et al. Numerical simulation of shrub roots for slope protection effects on loess area of Northeast Qinghai-Tibetan Plateau. *Chin. J. Rock. Mech Eng.* **29**, 1877–1884 (2010).
20. Li, Y. et al. Influence of the spatial layout of plant roots on slope stability. *Ecol. Eng.* **91**, 477–486. https://doi.org/10.1016/j.ecoleng.2016.02.026 (2016).
21. Świtała, B. M. & Wu, W. Numerical modelling of rainfall-induced instability of vegetated slopes. *Géotechnique* **68**(6), 481–491 (2018).
22. Cislaghi, A., Bordoni, M., Meisina, C. & Bischetti, G. B. Soil reinforcement provided by the root system of grapevines: Quantification and spatial variability. *Ecol. Eng.* **109**, 169–185. https://doi.org/10.1016/j.ecoleng.2017.04.034 (2017).
23. Huang, J. K., Wang, X. L., Ji, J. N., Chen, L. H. & Zhang, Z. W. Numerical simulation of root reinforcement for herbs in Loess Plateau based on asymptotic homogenization theory. *Trans. Chin. Soc. Agric. Eng.* **36**, 168–176 (2020).
24. Guang-Hui, C., Ling, W., Xu, O. & Han, J. Three-dimensional dynamic stability analysis of vegetation-rooted slopes. *Bull. Eng. Geol. Environ.* **83**, 483. https://doi.org/10.1007/s10064-024-03984-4 (2024).
25. Xia, Z., Yang, W., Dongrong, L. I., Jing, J. & Chaobo, Z. Strengthening effects of alfalfa roots on soil shear resistance in loess region. *Sci. Soil Water Conserv.* **17**(2), 53–59 (2019).
26. Xu, T. et al. Mechanical effects of vegetation protection on slope under loading conditions in loess areas of Xining Basin. *Trans. Chin. Soc. Agric. Eng.* **37**(02), 142–151 (2021).
27. Guo, H., Ng, C. W. W. & Zhang, Q. Three-dimensional numerical analysis of plant-soil hydraulic interactions on pore water pressure of vegetated slope under different rainfall patterns. *J. Rock Mech. Geotech. Eng.* **16**, 3696–3706. https://doi.org/10.1016/j.jrmge.2023.09.032 (2024).
28. Zhong, C., Cui, P., Zhu, S., Qing, Y. & Wu, L. Analysis of the influence of root water absorption on the stability of unsaturated soils slope. *JSWC* **36**, 99–105. https://doi.org/10.13870/j.cnki.stbcxb.2022.02.013 (2022).
29. Kokutse, N. K., Temgoua, A. G. T. & Kavazović, Z. Slope stability and vegetation: Conceptual and numerical investigation of mechanical effects. *Ecol. Eng.* **86**, 146–153 (2016).
30. Löbmann, M. T. et al. The influence of herbaceous vegetation on slope stability–a review. *Earth Sci. Rev.* **209**, 103328 (2020).
31. Chen, Q., Yang, X. & Zhou, J. Assessing the mechanical effects of vegetation on the stability of slopes with different geometries and soil types. *Bull. Eng. Geol. Env.* **83**(1), 8 (2024).
32. Van Genuchten, M. T. A closed-form equation for predicting the hydraulic conductivity of unsaturated soils. *Soil Sci. Soc. Am. J.* **44**(5), 892–898 (1980).
33. Wu, T. H., McKinnell Iii, W. P. & Swanston, D. N. Strength of tree roots and landslides on Prince of Wales Island, Alaska. *Can. Geotech. J.* **16**, 19–33. https://doi.org/10.1139/t79-003 (1979).
34. Xiao, S. & Li, S. Passive earth pressure of vegetation rooted soils based on limit analysis and quasi-static approach. *Comput. Geotech.* **150**, 104937. https://doi.org/10.1016/j.compgeo.2022.104937 (2022).
35. Bischetti, G. B. et al. Root strength and root area ratio of forest species in Lombardy (Northern Italy). *Plant Soil* **278**(1–2), 11–22 (2005).
36. Kumar, R., Shankar, V. & Jat, M. K. Evaluation of root water uptake models—a review. *ISH J. Hydraul. Eng.* **21**, 115–124. https://doi.org/10.1080/09715010.2014.981955 (2015).
37. Feddes, R. A., Kowalik, P., Kolinska-Malinka, K. & Zaradny, H. Simulation of field water uptake by plants using a soil water dependent root extraction function. *J. Hydrol.* **31**, 13–26. https://doi.org/10.1016/0022-1694(76)90017-2 (1976).
38. Han, K. et al. Initiation mechanism of shallow loess slope sliding under coupling effect of train vibration and rainfall. *Soil Dyn. Earthq. Eng.* **179**, 108556 (2024).
39. Zhang, Y., Pang, Q., Liu, Y. et al. Influence of root-soil complex characteristics of Amorpha Fruticosa on stability of loess slope. *Bull. Soil Water Conserv.* **44**(4) (2024).
40. Sun, P. et al. Field model experiments and numerical analysis of rainfall-induced shallow loess landslides. *Eng. Geol.* **295**, 106411. https://doi.org/10.1016/j.enggeo.2021.106411 (2021).
41. Xingsheng, L. et al. Progressive deformation and failure mechanism of loess fill slopes induce by rainfall: insights from flume model tests. *Bull. Eng. Geol. Environ.* https://doi.org/10.1007/S10064-023-03413-Y (2023).
42. Hu, J. et al. Quantifying the contribution of shrub roots to soil mechanical reinforcement using in situ shearing and assessing model reliability in coal mine subsidence areas, China. *CATENA* **246**, 108459. https://doi.org/10.1016/j.catena.2024.108459 (2024).
43. Song, X., Tan, Y. & Lu, Y. Microscopic analyses of the reinforcement mechanism of plant roots in different morphologies on the stability of soil slopes under heavy rainfall. *CATENA* **241**, 108018. https://doi.org/10.1016/J.CATENA.2024.108018 (2024).
44. Simon, A. & Collison, C. J. A. Quantifying the mechanical and hydrologic effects of riparian vegetation on streambank stability. *Earth Surf. Proc. Land.* **27**(5), 527–546. https://doi.org/10.1002/esp.325 (2002).
45. Xue, L. et al. Shallow slope stabilization by arbor root Systems: A physical model study. *CATENA* **246**, 108458. https://doi.org/10.1016/J.CATENA.2024.108458 (2024).

Acknowledgements

We acknowledge the support received from the research project (2023YJ231) of China Academy of Railway Sciences Co., LTD.

Author contributions

Conceptualization, K.K., D.Z., C.Y. and C.F.; methodology, K.K. and D.Z.; software, D.Z.; validation, K.K., W.Z. and D.Z.; formal analysis, D.Z. and C.Y.; investigation, D.Z.; resources, K.K. and D.Z.; data curation, D.Z.; writing—original draft preparation, D.Z.; writing—review and editing, D.Z. and C.Y.; visualization, W.Z. and D.Z.; supervision, K.K.; project administration, K.K. and C.F.; funding acquisition, K.K. and C.F. All authors have read and agreed to the published version of the manuscript.

Funding

This research was funded by China Academy of Railway Sciences Co., LTD, grant number 2023YJ231.

Declarations

Competing interests

The authors declare no competing interests.

Additional information

Correspondence and requests for materials should be addressed to Z.D.

Reprints and permissions information is available at www.nature.com/reprints.

Publisher's note Springer Nature remains neutral with regard to jurisdictional claims in published maps and institutional affiliations.